

Magnetic ordering and exchange effects in the antiferromagnetic solid solutions $\text{Mn}_x\text{Ni}_{1-x}\text{O}$

A. K. Cheetham and D. A. O. Hope*

Chemical Crystallography Laboratory, 9 Parks Road, Oxford OX1 3PD, England

(Received 1 July 1982; revised manuscript received 29 September 1982)

The antiferromagnetic phases of MnO, NiO, and the solid solutions $\text{Mn}_x\text{Ni}_{1-x}\text{O}$ ($x = 0.24, 0.48, 0.77$) have been examined by high-resolution powder neutron diffraction. The solid solutions have random cation distributions, and Néel temperature and mean cation-moment measurements indicate that the spins of Mn^{2+} and Ni^{2+} are effectively collinear owing to the strength of the 180° cation-anion-cation superexchange. As in MnO and NiO, the magnetic moments are confined to (111) planes by dipole-dipole forces, and the very small trigonal exchange strictions are interpreted in terms of a competition between antiferromagnetic $\text{Mn}^{2+}\text{-Mn}^{2+}$ and ferromagnetic $\text{Ni}^{2+}\text{-Mn}^{2+}$ nearest-neighbor exchange interactions.

I. INTRODUCTION

The insulating transition-metal oxides MnO and NiO adopt the cubic sodium chloride structure in their paramagnetic phases, and become antiferromagnetically ordered below Néel temperatures (T_N) of 118 K (Ref. 1) and 523 K (Ref. 2), respectively. Their magnetic and structural properties in the ordered states are ostensibly very similar; they have the same magnetic structure and easy plane,³ and experience rhombohedral ($\alpha > 90^\circ$) distortions at low temperatures.^{4,5} The magnetic structure consists of ferromagnetic (111) sheets, with adjacent planes having opposite spin directions.⁶ Neither Ni^{2+} nor high-spin Mn^{2+} have first-order orbital contributions, and the most important magnetic anisotropy term arises from the dipole-dipole interaction which restricts the moments to directions parallel to the (111) planes. The moment direction within these planes is selected by much weaker terms; that of MnO is unknown,^{7,8} while x-ray and neutron topography measurements⁹ indicate that the easy axis of NiO is [112]. Although the magnetic symmetry of both oxides is monoclinic, the readily observable deviations from cubic symmetry below T_N reflect only the trigonal configurational symmetry of the magnetic structure. The distortions are termed "exchange strictions," in contrast with the large magnetostrictive distortions of ferrous and cobaltous oxides which contain ions with orbitally degenerate ground states.

The magnetic structure is such that all exchange interactions between next-nearest neighbors (NNN) are antiferromagnetic, reflecting the importance of the 180° cation-oxygen-cation superexchange in these compounds. This interaction involves the e_g orbitals of the transition-metal ions and, according to the rules of superexchange coupling,¹⁰ is antiferromagnetic regardless of whether Ni^{2+} or Mn^{2+} is involved.

The other important superexchange pathways are those involving the nearest neighbors (NN); these are the 90° cation-oxygen-cation and cation-cation interactions.

In MnO, all exchange pathways are antiferromagnetic since every d orbital of Mn^{2+} is half-filled, and the large exchange striction appears to stem from attractive cation-cation exchange between ions in adjacent ferromagnetic planes, and a repulsion between ions in the same plane. No direct cation-cation exchange can take place in NiO since the t_{2g} orbitals are full, but 90° cation-anion-cation NN interactions can occur via the oxygen $2s$ and $2p$ orbitals. Both antiferromagnetic and ferromagnetic interactions are thereby predicted,¹⁰ but the sensitivity of the superexchange via oxygen $2s$ to interionic distance appears to be the cause of the $\alpha > 90^\circ$ exchange striction.

MnO and NiO are miscible in all proportions,¹¹ and magnetic susceptibility data have been obtained for $\text{Mn}_x\text{Ni}_{1-x}\text{O}$ with $x < 0.5$.¹² These show a decrease in $|\Theta|/T_N$ towards the composition $x = 0.5$ (indicative of an increase in ferromagnetic coupling) and an approximately linear dependence of T_N upon x . The use of high-resolution powder neutron diffraction in the investigation of the spin and crystallographic structures in the $\text{Mn}_x\text{Ni}_{1-x}\text{O}$ phase diagram will now be described.

II. EXPERIMENTAL

The mixed crystals were prepared by grinding together the requisite amounts of MnO and NiO in an agate mortar, pelleting, and firing at 1000°C for 24 h. A static vacuum was employed, and the samples were contained in alumina boats lined with platinum foil. The firings were repeated until adequate sample homogeneities were obtained. The sample quality

TABLE I. Lattice parameters, isotropic overall temperature factors, mean cation moments, and R factors for $\text{Mn}_x\text{Ni}_{1-x}\text{O}$ at 5 K.

Composition	Wavelength λ (Å)	a ($= b = c$) (Å)	α	β (deg)	γ	B_{overall} (Å ²)	$\bar{\mu}$ (μ_B)	R_{pr} ^a
NiO	1.510	8.3408(3)	90.08(1)	90.08(1)	90.08(1)	0.07(2)	1.90(6)	6.89
$\text{Mn}_{0.24}\text{Ni}_{0.76}\text{O}$	1.510	8.4756(4)	90.05(1)	90.05(1)	90.05(1)	0.23(2)	2.53(3)	4.76
$\text{Mn}_{0.48}\text{Ni}_{0.52}\text{O}$	1.905	8.6068(4)	90.04(1)	90.04(1)	90.04(1)	0.55(7)	3.16(3)	5.32
$\text{Mn}_{0.77}\text{Ni}_{0.23}\text{O}$	1.510	8.7697(3)	90.14(1)	90.14(1)	89.86(1)	0.54(2)	3.91(6)	7.84
MnO	1.510	8.8630(3)	90.60(1)	90.60(1)	90.60(1)	0.25(2)	4.58(3)	7.04

^a R_{pr} is the profile reliability index, as defined in Ref. 14.

was assessed by powder x-ray diffraction and analytical electron microscopy,¹³ and the manganese:nickel ratios were checked by atomic absorption spectrometry. Manganous oxide was obtained by decomposing manganous oxalate under a stream of hydrogen at 1000 °C, and Specpure nickel oxide was obtained from Johnson-Matthey Ltd.

Powder neutron-diffraction data at 5 K were collected for MnO, NiO, and three $\text{Mn}_x\text{Ni}_{1-x}\text{O}$ samples on the D1A diffractometer at the Institut Laue-Langevin, Grenoble, using wavelengths of 1.510 and 1.905 Å. The samples (8 g) were contained in vanadium cans held in an aluminum-tailed cryostat, and the time for a typical scan ($0^\circ < 2\theta < 160^\circ$) was 12–24 h. A variable temperature scan of the {111} peak of a manganese-rich solid solution was also carried out. The data were analyzed by the profile-analysis technique of Rietveld¹⁴ using trigonal unit cells, and the scattering lengths of Mn, Ni, and oxygen were taken from Bacon.¹⁵ Peaks occurring at $2\theta < 25^\circ$ were omitted from the analyses owing to large deviations from a Gaussian peak shape at these angles, and an asymmetry correction was applied in the range $25^\circ < 2\theta < 48^\circ$. The form factors determined previously for MnO (Ref. 16) and NiO (Ref. 17) were applied to these data sets, and no improvement was obtained from different expansions of the free-ion form factors. Since a variety of factors contribute to the form-factor curve, those applied to the solid-solution data were determined empirically, using indications from the profile reliability index. The results are set out in Table I; The parameters for MnO and NiO are very similar to those determined previously by diffraction methods.^{4, 5, 16, 18}

III. RESULTS AND DISCUSSION

At 5 K, the solid-solution powder profiles show only magnetic peaks characteristic of the magnetic

structure of the end members. There is no evidence for long-range ordering of nickel and manganese, which would be readily detected by neutron diffraction owing to the appreciable difference between the scattering lengths of the two elements (Mn, -0.372×10^{-14} m; Ni, 1.03×10^{-14} m).

The {111} magnetic superlattice peak of $\text{Mn}_{0.77}\text{Ni}_{0.23}\text{O}$ was monitored as a function of increasing temperature, and disappeared above $T_N = 210 \pm 5$ K. This value is in good agreement with the data of Aivazov and Gurov,¹² and the linear dependence of T_N upon composition indicates that a noncollinear “oblique antiferromagnetic” (OAF) phase¹⁹ does not occur in this system. OAF behavior has been observed in two-dimensional magnetic systems [e.g., $\text{Fe}_x\text{Co}_{1-x}\text{Cl}_2$,²⁰ $\text{K}_2\text{Fe}_x\text{Mn}_{1-x}\text{F}_4$ (Ref. 21)], where the anisotropies of the components dominate the exchange; the reverse must be the case in $\text{Mn}_x\text{Ni}_{1-x}\text{O}$.

The linear variation of the mean sublattice moment of $\text{Mn}_x\text{Ni}_{1-x}\text{O}$ with composition (Fig. 1) is also compatible with effectively collinear moments for Mn^{2+} and Ni^{2+} . These values were obtained by calculating

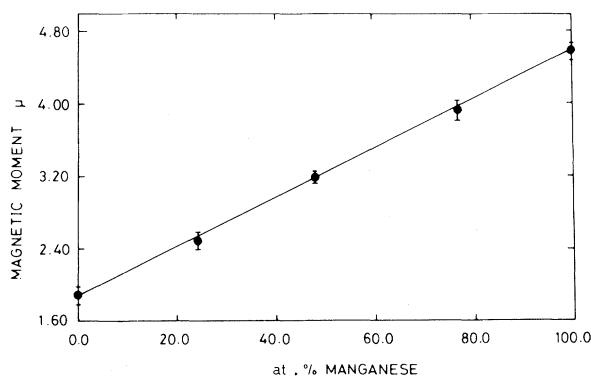


FIG. 1. Mean sublattice moments of the solid solutions $\text{Mn}_x\text{Ni}_{1-x}\text{O}$ at 5 K.

structure factors according to the magnetic structure adopted by MnO and NiO. Similar results have been reported in the system NiO-CoO.²² The best profile residuals are listed in Table I and were obtained with the moments located within (111) planes indicating that, as in the end members, the dipolar forces constitute the most important anisotropic contribution. For samples with $x = 0, 0.24, 0.48, 1.0$, the uniaxial configurational symmetry²³ does not allow any deductions to be made as to the moment direction within the (111) plane. In $\text{Mn}_{0.77}\text{Ni}_{0.23}\text{O}$, the symmetry is lower (see below) but the profile analyses were very insensitive to different spin directions within the easy plane.

The lattice parameters set out in Table I reveal that

the exchange strictions of all the solid solutions are much smaller than those predicted by a linear interpolation between NiO ($\alpha = 90.08^\circ$) and MnO ($\alpha = 90.60^\circ$), an observation illustrated by inspection of the high-angle regions of the profiles of two compositions (Fig. 2). In $\text{Mn}_x\text{Ni}_{1-x}\text{O}$, the small peak splittings are evidence for symmetries very close to cubic, and it seems that, in the solid solutions, the $\alpha > 90^\circ$ distortions characteristic of MnO and NiO (stemming from antiferromagnetic NN interactions) are opposed by an appreciable $\alpha < 90^\circ$ striction due to ferromagnetic exchange between unlike ions. By analogy with the large distortion of MnO itself, such a large effect can be associated with the cation-cation exchange between Ni^{2+} and Mn^{2+} , which involves the

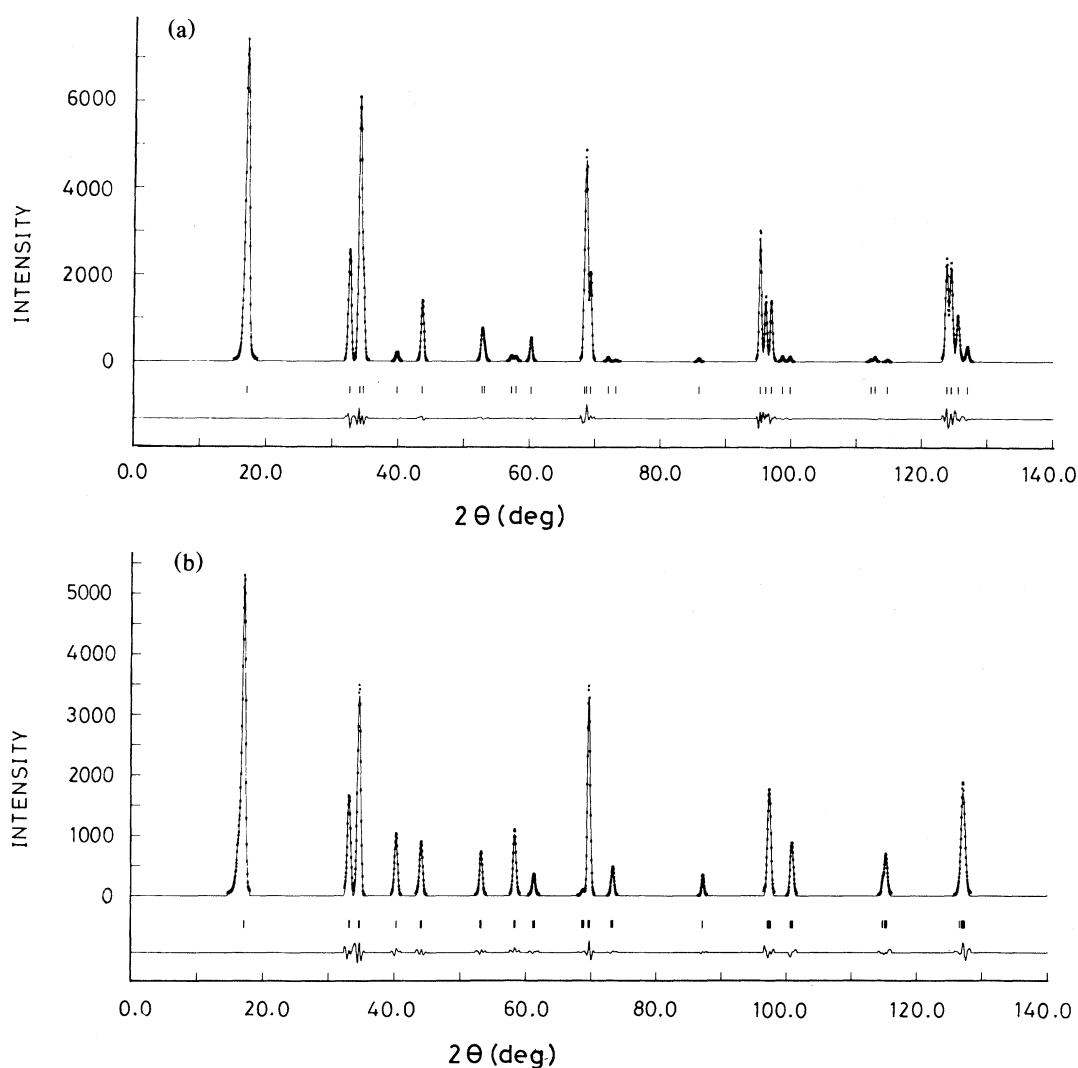


FIG. 2. Observed (crosses) and calculated (full line) profiles of $\text{Mn}_x\text{Ni}_{1-x}\text{O}$ (a) $x = 1.0$, (b) $x = 0.77$, at 5 K. Difference profiles are also shown and reflection positions are marked. The asymmetric [111] peak was not included in refinements. Note the dramatic difference in the peak splittings between (a) and (b).

virtual transfer of electrons between the t_{2g} orbitals of nearest neighbors. Mn^{2+} is a high-spin ion in oxides because the intra-ionic exchange stabilization Δ_{ex} is larger than the cubic crystal-field splitting, Δ_c , and in ferromagnetic Ni^{2+} - Mn^{2+} exchange a β -spin Ni^{2+} electron is transferred in order that the loss of intra-ionic exchange of Ni^{2+} is minimized. An antiferromagnetic alignment of the Ni^{2+} and Mn^{2+} spins would involve the exchange of a Ni^{2+} t_{2g} α -spin electron, which has the additional stabilization Δ_{ex} . It is noteworthy that these results support the observed decrease in $|\Theta|/T_N$ upon solid-solution formation.

Table I shows that optimum refinements of the data from $Mn_{0.77}Ni_{0.23}O$ were obtained with a pseudocubic cell having $a = b = c$, $\alpha = \beta > 90^\circ$, $\gamma < 90^\circ$. Refinements with $\alpha = \beta = \gamma < 90^\circ$ and $\alpha = \beta = \gamma > 90^\circ$ furnished R_{pr} values of 10.7% and 10.9%, respectively, compared with 7.8% obtained

with the former lattice parameters, and it seems that in this case the magnetic structure does not propagate along a threefold axis of the pseudocube. Assuming a single-axis magnetic structure of the MnO type, the cause of this behavior is unclear.

ACKNOWLEDGMENTS

We are grateful to Professor J. B. Goodenough and Dr. P. D. Battle for some helpful discussions, Dr. A. W. Hewat and Dr. C. Wilkinson for their assistance at the Institut Laue-Langevin, Mrs. A. Stoker for the electron microscopy analyses, the United Kingdom Science and Engineering Research Council for the provision of neutron facilities and a studentship to D.A.O.H., and the U.S. Air Force for Research Grant No. AFOSR 79-0120.

*Now at Royal Signals and Radar Establishment, St. Andrews Road, Great Malvern, Worcester WR14 3PS, England.

¹R. Boire and M. F. Collins, *Can. J. Phys.* **55**, 688 (1977).

²C. H. La Blanchetais, *J. Phys. Radium* **12**, 765 (1951).

³W. L. Roth, *Phys. Rev.* **110**, 1333 (1958).

⁴B. Morosin, *Phys. Rev. B* **1**, 236 (1970).

⁵L. C. Bartel and B. Morosin, *Phys. Rev. B* **3**, 1039 (1971).

⁶C. G. Shull, W. A. Strauser, and E. O. Wollan, *Phys. Rev.* **83**, 333 (1951).

⁷R. Bidaux, R. Conte, and J. A. Nasser, *J. Appl. Phys.* **50**, 1683 (1979).

⁸R. Bidaux, R. Conte, and J. A. Nasser, *J. Phys.* **41**, 1317 (1980).

⁹J. Baruchel, M. Schlenker, K. Kurosawa, and S. Saito, *Philos. Mag. B* **43**, 853 (1981).

¹⁰J. B. Goodenough, *Magnetism and the Chemical Bond* (Wiley-Interscience, New York, 1963).

¹¹W. C. Hahn and A. Muan, *J. Phys. Chem. Solids* **19**, 338 (1961).

¹²M. I. Aivazov and S. V. Gurov, *Inorg. Mater.* **10**, 738 (1974).

¹³A. K. Cheetham and A. J. Skarnulis, *Anal. Chem.* **53**, 1060 (1981).

¹⁴H. M. Rietveld, *J. App. Crystallogr.* **2**, 65 (1969).

¹⁵G. E. Bacon, *Neutron Diffraction* (Oxford Univ. Press, London, 1975).

¹⁶A. J. Jacobson, B. C. Tofield, and B. E. F. Fender, *J. Phys. C* **6**, 1615 (1973).

¹⁷H. Alperin, *Phys. Rev. Lett.* **6**, 55 (1961).

¹⁸B. E. F. Fender, A. J. Jacobson, and F. A. Wedgewood, *J. Appl. Phys.* **48**, 990 (1968).

¹⁹K. Katsumata, M. Kobayashi, T. Sato, and Y. Miyako, *Phys. Rev. B* **19**, 2700 (1979).

²⁰T. Tawaraya and K. Katsumata, *Solid State Commun.* **32**, 337 (1979).

²¹L. Bevaart, E. Frikkee, J. V. Levesque, and L. J. de Jongh, *Phys. Rev. B* **18**, 3376 (1978).

²²P. D. Battle, A. K. Cheetham, and G. A. Gehring, *J. Appl. Phys.* **50**, 7578 (1979).

²³G. Shirane, *Acta Crystallogr.* **12**, 282 (1959).